

1

=enter title here=

2

=list all authors here=

3

=number= =Affiliation Address=

4

**Key Points:**

5

- enter point 1 here
- enter point 2 here
- enter point 3 here

6

7

---

Corresponding author: =name=, =email address=

8      **Abstract**

9      enter abstract here

10     **1 Introduction**

11    Slow slip events are a new feature discovered in the last two decades in many sub-  
 12   duction zones thanks to recordings of the displacement of Earth's surface by dense Global  
 13    Navigation Satellite System (GNSS) networks. As with ordinary earthquakes, slow slip  
 14    events are caused by slip on a fault, such as the plate boundary between a tectonic plate  
 15    subducting under another tectonic plate. However, they take a much longer time (sev-  
 16    eral days to several years) to happen relative to ordinary earthquakes, and they have a  
 17    relatively short recurrence time (months to years), compared to the recurrence time of  
 18    regular earthquakes (up to several hundreds of years), allowing scientists to observe and  
 19    study many complete event cycles, which is typically not possible to explore with tra-  
 20    ditional earthquake catalogs (Beroza & Ide, 2011). A slow slip event on the plate bound-  
 21    ary is inferred to happen when there is a reversal of the direction of motion at GNSS sta-  
 22    tions, compared to the secular interseismic motion. Slow slip events have been observed  
 23    in many subduction zones, such as Cascadia, Nankai (southwest Japan), Alaska, Costa  
 24    Rica, Mexico, and New Zealand (Audet & Kim, 2016; Beroza & Ide, 2011).

25    In many places, tectonic tremor are also observed in relation to slow slip. Tremor  
 26    is a long (several seconds to many minutes), low amplitude seismic signal, with emer-  
 27    gent onsets, and an absence of clear impulsive phases. Tectonic tremor have been explained  
 28    as a swarm of small, low-frequency earthquakes (LFEs) (Shelly, Beroza, & Ide, 2007),  
 29    that is small magnitude earthquakes ( $M \sim 1$ ), for which frequency content (1-10 Hz) is  
 30    lower than for ordinary earthquakes (up to 20 Hz). In subduction zones such as Nankai  
 31    and Cascadia, tectonic tremor observations are spatially and temporally correlated with  
 32    slow slip observations (Obara, 2002; Rogers & Dragert, 2003). Due to this correlation,  
 33    these paired phenomena have been called Episodic Tremor and Slip (ETS). However, this  
 34    is not always the case. For instance, in northern New Zealand, tremor are more challeng-  
 35    ing to detect, and seem to be located downdip of the slow slip on the plate boundary.

36    In Cascadia and Guerrero, Mexico, tremor has been used as a proxy to observe slow  
 37    slip events that are not directly detectable in the GNSS data. For instance, Aguiar, Mel-  
 38    bourne, and Scrivner (2009) computed the GPS-estimated moment release for 23 ETS  
 39    events in Cascadia between 1997 and 2008. Simultaneously, they computed the cumu-  
 40    lative number of hours of tectonic tremor recorded for each event. They observed a lin-  
 41    ear relationship between moment release and number of hours of tremor for ETS events  
 42    of moment magnitude 6.3 to 6.8. For all these events, at least 50 hours of tectonic tremor  
 43    where observed simultaneously with the GPS deformation. However, many smaller bursts  
 44    of tremor of duration 1 to 50 hours were also observed in between the big ETS events.  
 45    Based on the relationship between slow slip moment and number of hours of tremor, Aguiar  
 46    et al. (2009) suggested that smaller slow slip events of magnitude 5-6 may occur simul-  
 47    taneously with the tremor bursts without being detectable in the GPS data.

48    Frank (2016) transformed the GPS time series into daily increments of surface mo-  
 49    tion by computing the first order differentiation of the time series. He then discarded  
 50    the daily increments observed during known big slow slip events, and focused on the inter-  
 51    events period. He divided the daily increments into two groups: the first group contains  
 52    days when slow seismicity (tectonic tremor and LFEs) is detected, the second group con-  
 53    tains days when the numbers of LFEs (for Guerrero) or tremor (for Cascadia) is lower  
 54    than a threshold. He then stacked separately the two groups of daily increments and ob-  
 55    served a cumulative displacement in the northern direction (for Guerrero) and the east-  
 56    ern direction (for Cascadia) corresponding to the loading period when few tremor or LFEs  
 57    are observed and the surface deformation corresponds to the secular plate motion. He  
 58    also observed a cumulative displacement in the southern direction (for Guerrero) and  
 59    the western direction (for Cascadia) corresponding to the release period when tremor

60 and LFEs are observed. This reverse displacement corresponds to smaller slow slip events  
 61 not directly observable in the GPS data.

62 However, in other subduction zones such as New Zealand, there is no clear relationship  
 63 between tremor and slow slip occurrence and these methods cannot be applied.  
 64 We thus need other methods to be able to better detect and quantify slow slip.

65 Wavelets methods such as the Discrete Wavelet Transform (DWT) are mathematical  
 66 tools for analyzing time series simultaneously in the time and the frequency domain  
 67 by observing how weighted averages of a time series vary from one averaging period to  
 68 the next. Wavelet methods have been widely used for geophysical applications (Kumar  
 69 & Foufoula-Georgiou, 1997). However, few studies have used wavelet methods to analyze  
 70 recordings of slow slip, and their scope was limited to the detection of the bigger  
 71 (magnitude 6-7) short-term (a few weeks) events.

72 Alba, Weldon, Livelybrooks, and Schmidt (2019) used hourly water level records  
 73 from four tide gauges in the Juan de Fuca Straight and the Puget Sound to determine  
 74 vertical displacements, uplift rates between ETS events, and net uplift rates between 1996  
 75 and 2011. The noise in the tide gauges data is associated with tides, and ocean and at-  
 76 mospheric noise on multiple timescales (a few days for storms to decades for oscillations  
 77 between ocean basins), and is assumed to be coherent between each of the four tidal gauges  
 78 studied. On the contrary, the uplift due to ETS events should be different at each tidal  
 79 gauge. They first removed the tides using NOAA hourly harmonic tidal predictions. They  
 80 then removed the residual noise using a method based on the DWT. More precisely, the  
 81 authors applied a DWT to each of the four sites studied, and to the average of the four  
 82 sites. Then, for each level of the DWT decomposition, they carried out a linear regres-  
 83 sion between the detail for one site and the detail for the average of the four sites. This  
 84 process gives a coefficient for each level and for each site. They then constructed a noise  
 85 signal for each site by multiplying the coefficient from the linear regression by the de-  
 86 tail of the average over the four sites, and summing for all levels. The noise signal thus  
 87 obtained was then removed from the time series. They then stacked multiple events to  
 88 obtain an average event uplift rate, aligning the 12 ETS events using exact timing from  
 89 GPS data. A difference in uplift between the two tidal gauges at Port Angeles and Port  
 90 Townsend was then clearly seen in the stacked time series. Finally, the authors removed  
 91 the long-term uplift rate and the long-term sea level rise to obtain an average inter-event  
 92 uplift rate. They found that the inter-event deformation at a site is equal and opposite  
 93 to the deformation during an ETS event, suggesting that ETS events are, on average,  
 94 releasing the strain accumulated between ETS events.

95 Szeliga, Melbourne, Santillan, and Miller (2008) determined the timing and the  
 96 amplitude of 34 slow slip events throughout the Cascadia subduction zone between 1997  
 97 and 2005. They stabilized the GPS time series using a reference set of stations from sta-  
 98 ble North America. They then modelled the GPS time series by the sum of a linear trend,  
 99 annual and biannual sinusoids representing seasonal effects, and Heaviside step functions  
 100 corresponding to earthquakes and hardware upgrades. The linear system was then solved  
 101 using a weighted QR decomposition. Finally, they applied a Gaussian wavelet transform  
 102 to the residual time series to get the exact timing of the slow slip at each GPS station.  
 103 The succeeding wavelet basis functions are increasingly sensitive to temporal localiza-  
 104 tion of a given signal, and the onset of faulting appears on the wavelet spectrum as an  
 105 amplitude spike present over all frequencies. The offset for each slow slip event was then  
 106 used to invert for the slow slip at depth by assuming a thrust fault slip at each subfault  
 107 of the plate boundary. An equivalent moment magnitude was thus obtained.

108 Finally, instead of using wavelets in the time domain, Ohtani, McGuire, and Segall  
 109 (2010) used 2D wavelet functions in the spatial domain to detect slow slip events. They  
 110 designed the Network Stain Filter (NSF) to detect transient deformation signals from  
 111 large-scale geodetic arrays. Contrary to their previous work on the Network Inversion  
 112 Filter (NIF), there is no need to specify potential sources of deformation. They mod-  
 113 elled the position of the GPS station by the sum of the secular velocity, a spatially co-  
 114 herent field, site-specific noise, reference frame errors, and observation errors. The spa-

115       tial displacement field is modeled by the sum of basis wavelets (the Deslauriers-Dubuc  
 116       wavelet of degree 3) with time-varying weights. The transient is considered to be nearly  
 117       steady-state, so that it has spatial weights for the displacement and the velocity, but the  
 118       acceleration is modeled by a random walk with a time-varying variance. All the time varying  
 119       coefficients are estimated using Kalman filtering, and the optimization problem is  
 120       regularized with the spatial sum of the transient strain rate field. Their method has been  
 121       successfully used to detect a transient event in the Boso peninsula, Japan, and a slow  
 122       slip event in the Alaska subduction zone (Wei, McGuire, & Richardson, 2012).

123       In this study, we use wavelet methods to analyze GPS and seismic recordings of  
 124       slow slip events in Cascadia. Our objective is to verify that there is a good correlation  
 125       between slow slip events detected with only GNSS data, and slow slip events detected  
 126       with only seismic data. We thus want to demonstrate that the wavelet-based detection  
 127       method can be applied to detect slow slip events that may be currently undetected with  
 128       standard methods.

## 129       2 Data

130       We focused our study on northwest Washington State. For the GNSS data, we used  
 131       the GPS time series provided by the Pacific Northwest Geodetic Array, Central Wash-  
 132       ington University. These are network solutions in ITRF2008 with phase ambiguities re-  
 133       solved. Solutions are computed with JPL/NASA orbits and satellite clocks. North, East,  
 134       and Vertical directions are available. However, as the direction of the secular plate mo-  
 135       tion is close to the East direction, we only used the East direction of the GPS time se-  
 136       ries for the data analysis, as it has the best signal-to-noise ratio. The wavelet method  
 137       works best with data with zero mean, and no sharp discontinuities, so we use the cleaned  
 138       dataset, that is GPS times eries with linear trends, steps due to earthquakes or hard-  
 139       ware upgrades, and annual and semi-annual sinusoids signals simultaneously estimated  
 140       and removed following Szeliga, Melbourne, Miller, and Santillan (2004). For the seis-  
 141       mic data, we used the tremor catalog from the Pacific Northwest Seismic Network (PNSN)  
 142       (Wech, 2010). Tremor were detected and located using waveform envelope correlation  
 143       and clustering and a centroid location is available for every given five-minute time win-  
 144       dow when tremor was detected. As the catalog starts in August 2009, we only looked  
 145       at GPS data recorded in 2009 or later.

## 146       3 Method

### 147       3.1 The Maximal Overlap Discrete Wavelet Transform

148       The Discrete Wavelet Transform (DWT) is an orthonormal transform that trans-  
 149       forms a time series  $X_t$  ( $t = 0, \dots, N - 1$ ) into a vector of wavelet coefficients  $W_i$  ( $i = 0, \dots, N - 1$ ).  
 150       If we denote  $J$  the level of the wavelet decomposition, and we have  $N = n * 2^J$ , where  
 151        $n$  is some integer higher or equal to 1, the vector of wavelet coefficients can be decom-  
 152       posed into  $J$  wavelet vectors  $W_j$  of lengths  $\frac{N}{2}, \frac{N}{4}, \dots, \frac{N}{2^J}$ , and one scaling vector  $V_J$  of  
 153       length  $\frac{N}{2^J}$ . Each wavelet vector  $W_j$  is associated with changes on scale  $\tau_j = dt2^{j-1}$ , where  
 154        $dt$  is the time step of the time series, and corresponds to the filtering of the original time  
 155       series with a filter with nominal frequency interval  $[\frac{1}{dt2^{j+1}}, \frac{1}{dt2^j}]$ . The scaling vector  $V_J$   
 156       is associated with averages in scale  $\lambda_J = dt2^J$ , and corresponds to the filtering of the  
 157       original time series with a filter with nominal frequency interval  $[0, \frac{1}{dt2^{j+1}}]$ . We can also  
 158       define for  $j = 1, \dots, J$  the  $j$ th wavelet detail  $D_j$ , which is a vector of length  $N$ , and  
 159       is associated to scale  $\tau_j = dt2^{j-1}$ . Similarly, we can define for  $j = 1, \dots, J$  the  $j$ th  
 160       wavelet smooth  $S_j$ , which is a vector of length  $N$ , and is associated to scales  $\tau_{j+1} = dt2^{j+1}$   
 161       and higher. Together, the details and the smooths define the multiresolution analysis (MRA)  
 162       of  $X$ :

$$X = \sum_{j=1}^J D_j + S_J \quad (1)$$

The DWT present several disadvantages. First, the length of the time series must be a multiple of  $2^J$  where  $J$  is the level of the DWT decomposition. Second, the time step of the wavelet vector  $W_j$  is  $dt2^j$ , which may not correspond to the time when some interesting phenomenon is visible on the original time series. Third, when we circularly shift the time series, the corresponding wavelet coefficients, details and smooths are not a circularly shifted version of the wavelet coefficients, details and smooths of the original time series. Thus, the values of the wavelet coefficients, details and smooths are strongly dependent on the time when we start experimentally gathering the data. Finally, when we filter the time series to obtain the details and smooths, we introduce a phase shift, which makes difficult to line up meaningfully the features of the MRA with the original time series.

This is why we use instead the Maximal Overlap Discrete Wavelet Transform (MODWT). The MODWT transforms the time series  $X_t$  ( $t = 0, \dots, N - 1$ ) into  $J$  wavelet vectors  $\tilde{W}_j$  ( $j = 1, \dots, J$ ) of length  $N$  and a scaling vector  $\tilde{V}_J$  of length  $N$ . As is the case for the DWT, each wavelet vector  $\tilde{W}_j$  is associated with changes on scale  $\tau_j = dt2^{j-1}$ , and corresponds to the filtering of the original time series with a filter with nominal frequency interval  $[\frac{1}{dt2^{j+1}}, \frac{1}{dt2^j}]$ . The scaling vector  $\tilde{V}_J$  is associated with averages in scale  $\lambda_J = dt2^J$ , and corresponds to the filtering of the original time series with a filter with nominal frequency interval  $[0; \frac{1}{dt2^{J+1}}]$ . As is the case for the DWT, we can write the MRA:

$$X = \sum_{j=1}^J \tilde{D}_j + \tilde{S}_J \quad (2)$$

The MODWT of a time series can be defined for any length  $N$ . The time step of the wavelet vectors  $\tilde{W}_j$  and the scaling vector  $\tilde{V}_J$  is equal to the time step of the original time series. When we circularly shift the time series, the corresponding wavelet vectors, scaling vector, details and smooths are shifted by the same amount. The details and smooths are associated with a zero phase filter, making it easy to line up meaningfully the features of the MRA with the original time series. The wavelet methods for time series analysis are explained in a more detailed way in Percival and Walden (2000)).

### 3.2 Application to synthetic data

To illustrate the wavelet transform method, we first apply the MODWT to synthetics data. As slow slip events occur in Cascadia on a regular basis, every twelve to eighteen months, we create a synthetic signal of period  $T = 500$  days. To reproduce the ground displacement observed on the longitudinal component of GPS stations in Cascadia, we divide each period into two parts: In the first part of duration  $T-N$ , the displacement is linearly increasing and corresponds to the secular plate motion in the eastern direction; in the second part of duration  $N$ , the displacement is linearly decreasing and corresponds to a slow slip event on a reverse fault at depth triggering a ground displacement in the western direction. To see the effect of the magnitude of the slow slip event, we use different values for  $N = 2, 5, 10, 20$  days. Figure 1 shows the synthetics, the details of the wavelet decomposition for levels 1 to 8, and the smooth for the four durations of a slow slip event.

The ramp-like signal is transformed through the wavelet filtering into a waveform with first a positive peak and then a negative peak. The width of the waveform increases with the scale level. For the 8th level of the wavelet decomposition, the width of the waveform is nearly as large as the time between two events. We do not show details at larger scales as the corresponding waveforms would start to merge two contiguous events to-

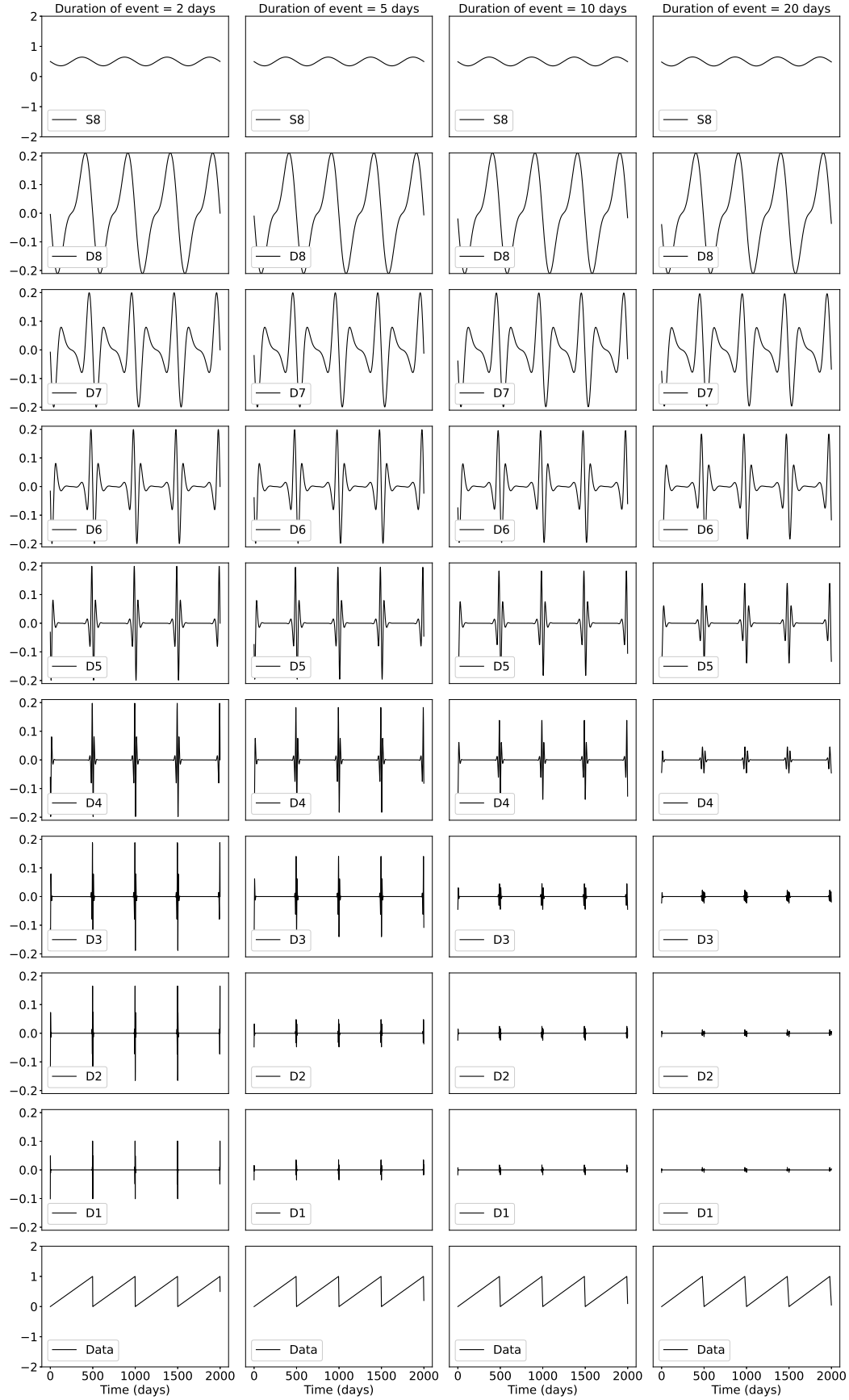


**Figure 1.** Details and smooth of the wavelet decomposition of a synthetics signal with period 500 days and duration of the slow slip event equal to 2 days (left), 5 days, 10 days, and 20 days (right).

209      gether, and make the wavelet decomposition less interpretable. For an event of duration  
 210      2 days, the wavelet details at levels higher than 2 have a larger amplitude than the wavelet  
 211      detail at level 1. For an event of duration 5 days, the wavelet details at levels higher than  
 212      3 have a larger amplitude than the wavelet details at lower scales. For an event of du-  
 213      ration 10 days, the wavelet details at levels higher than 5 have a larger amplitude than  
 214      the wavelet details at lower scales. For an event of duration 20 days, the wavelet details  
 215      at levels higher than 6 have a larger amplitude than the wavelet details at lower scales.  
 216      Thus, the scale levels at which an event is being seen in the wavelet details give us an  
 217      indication about the duration (and the magnitude) of the slow slip event. We expect the  
 218      big slow slip events of magnitude 6-7 that lasts about 10 days to start being visible at  
 219      the level 5 of the wavelet decomposition, but to not be noticeable at lower time scales.

### 220      3.3 MODWT of GPS and tremor data

221      The DWT and MODWT methods must be used on a continuous time series, with-  
 222      out gaps in the recordings. To deal with the gaps in the GNSS recordings, we simply re-  
 223      place the missing values by the sum of a straight line and a Gaussian noise component  
 224      with mean zero and standard deviation equal to the standard deviation of the whole time  
 225      series. The straight line starts at the mean of the five days before the gap and ends at  
 226      the mean of the five days after the gap. We verify how the wavelet details may be af-  
 227      fected by looking at a GPS time series without missing values and comparing the wavelet  
 228      details with and without removing some data points. Station PGC5 has recorded dur-  
 229      ing 1390 days between 2009 and 2013, without any missing values. We first computed  
 230      the wavelet details without missing values. Then, we removed ten neighboring missing  
 231      values, replaced them by the sum of the straight line and the Gaussian noise component,  
 232      and computed the wavelet details with the replaced values. Figure 2 shows a compar-  
 233      ison of the two wavelet details for two different locations of the missing values. We can  
 234      see that there are visible differences in the time series itself, and in the details at the small-  
 235      est levels of the wavelet decomposition. However, the differences between the wavelet de-  
 236      tails with and without missing values get smaller and smaller with increasing levels the  
 237      details, and are barely visible for the levels we are mostly interested in (levels 6 and above).  
 238      We thus conclude that we can easily replace the missing values in the GNSS time series  
 239      without introducing false detections of slow slip events.

240      We then applied the wavelet filtering to real GPS data. Figure 3 shows the longi-  
 241      tudinal displacement for GPS station PGC5, located in southern Vancouver Island, the  
 242      details of the wavelet decomposition for levels 1 to 8, and the smooth. In the data, we  
 243      can see a sharp drop in displacement whenever there is a slow slip event. For levels 5 to  
 244      8, we can see in the details a positive peak followed by a negative peak whenever there  
 245      is a drop in displacement in the data. We thus verify that the wavelet method can de-  
 246      tect slow slip events.

247      To increase the signal-to-noise ratio and be able to better detect slow slip events,  
 248      we stack the signal over several GPS stations. We choose to focus on GPS stations lo-  
 249      cated close enough to the tremor zone to get a sufficiently high amplitude of the slow  
 250      slip signal. We choose 16 points located on the 40 km depth contour of the plate bound-  
 251      ary (model from Preston, Creager, Crosson, Brocher, and Trehu (2003)) with spacing  
 252      equal 0.1 degree in latitude (red triangles on Figure 4). Then we took all the GPS sta-  
 253      tions located in a 50 km radius for a given point, compute the wavelet details for the lon-  
 254      gitudinal displacement of each station, and stack each detail over the GPS stations. We  
 255      thus have a stacked detail for each level 1 to 8 of the wavelet decomposition.

256      To compare slow slip events detected with GPS data and slow slip events detected  
 257      with seismic data, we took all the tremor epicenters located within a 50 km radius cen-  
 258      tered on one of the 16 locations marked by red triangles on Figure 3. Then we computed  
 259      the cumulative number of tremor within this circle. Finally, we removed a linear trend  
 260      from the cumulative tremor count, and applied the wavelet transform. Figure 5 shows  
 261      an example of the wavelet decomposition for the third northernmost location on Figure

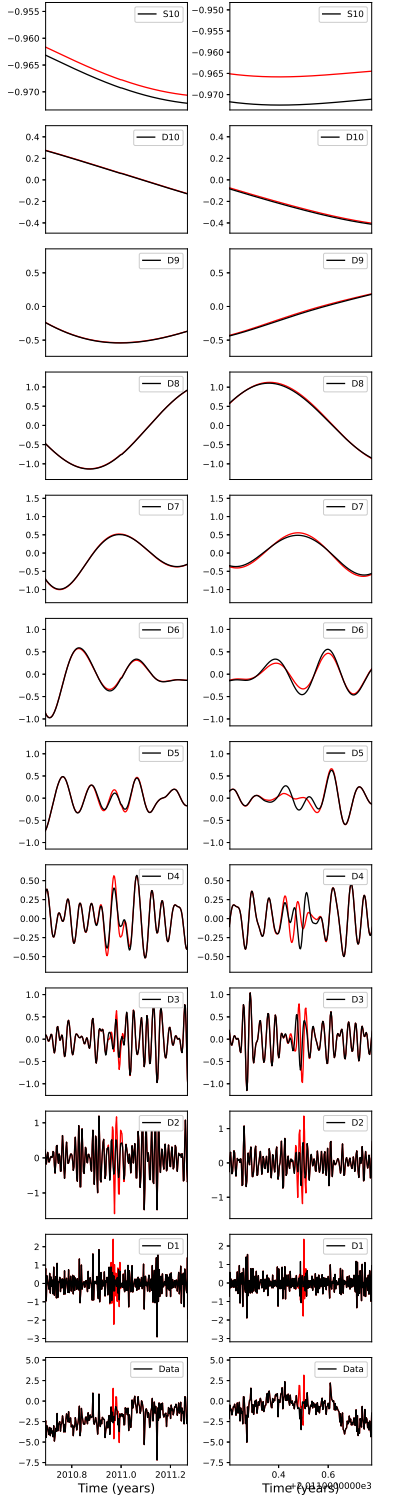


**Figure 2.** Bottom: Data from GPS station PGC5 without missing values (black) and with missing values replaced by the sum of a straight line and a Gaussian noise component (red) for two locations of the missing values (left and right). Bottom to top: Corresponding ten details and smooths of the wavelet composition for the original data (black) and for the missing values replaced by the sum of a straight line and a Gaussian noise component (red).

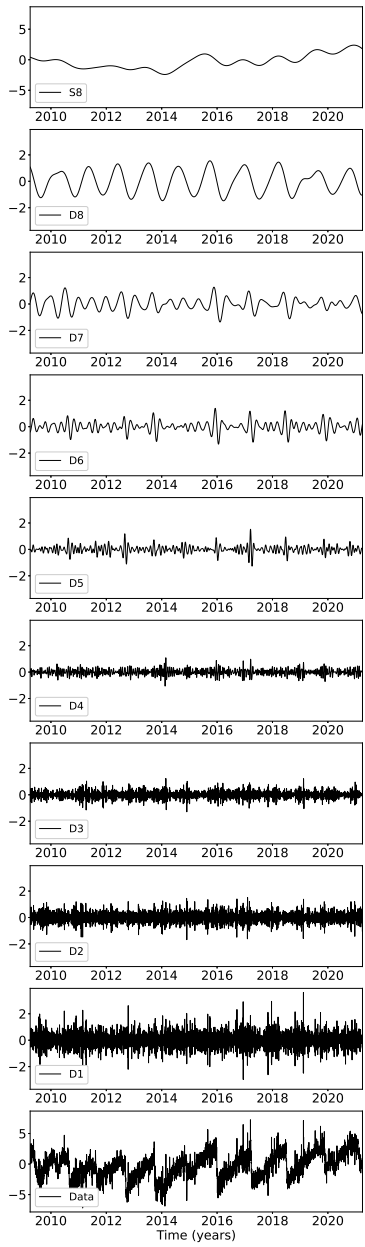


**Figure 3.** Details and smooth of the wavelet decomposition of the longitudinal displacement recorded at GPS station PGC5.

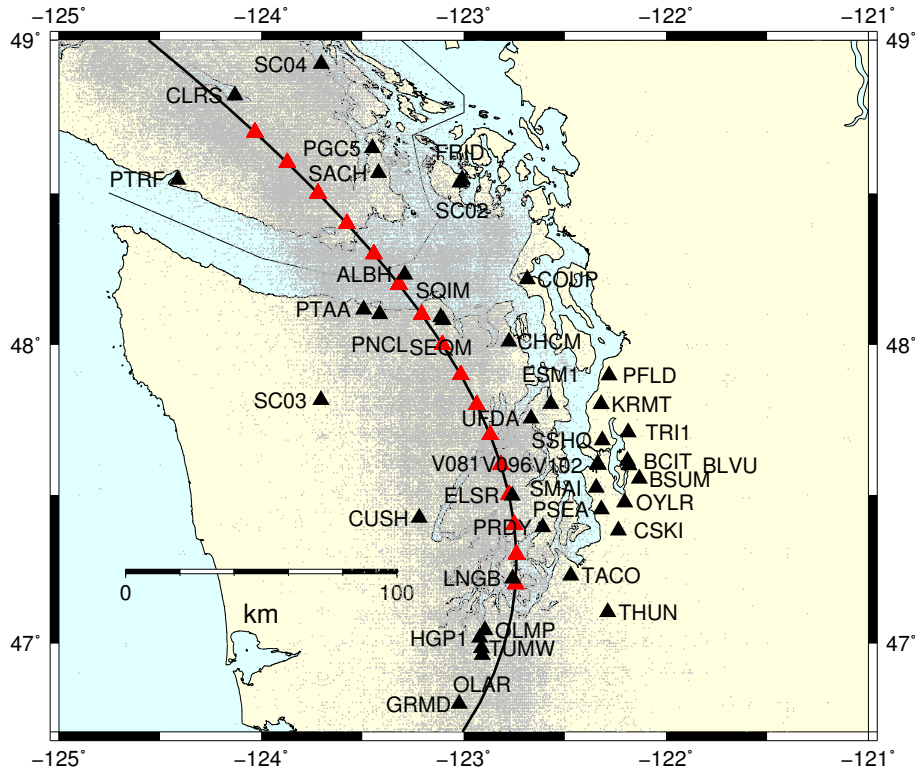


**Figure 4.** GPS stations used in this study (black triangles). The black line represents the 40 km depth contour of the plate boundary model by Preston et al. (2003). The red triangles are the locations where we stack the GPS data. The small grey dots are all the tremor locations from the PNSN catalog.

262 4 (which is closest to GPS station PGC5). Contrary to what happens for the GPS data,  
 263 we see a sharp increase in the data whenever there is a tremor episode, which translates  
 264 into a negative peak followed by a positive peak in the wavelet details.

## 265 4 Results

266 We stacked the 8th level detail of the wavelet decomposition of the displacement  
 267 over all the GPS stations located in a 50 km radius of a given point, for the 16 locations  
 268 indicated in Figure 3. The result is shown in the top panel of Figure 6, where each line  
 269 represents one of the locations. To better highlight the peaks in the wavelet details, we  
 270 highlighted in red the time intervals where the amplitude of the stacked detail is higher  
 271 than a threshold, and in blue the time intervals where the amplitude of the stacked de-  
 272 tail is lower than minus the threshold. To compare the GPS signal with the tremor sig-  
 273 nal, we plotted the 8th level detail of the wavelet decomposition of the tremor count on  
 274 the bottom panel of Figure 6. We used the opposite of the cumulative tremor count for  
 275 the wavelet decomposition in order to be able to match positive peaks with positive peaks  
 276 and negative peaks with negative peaks. Although the latitudinal extension of the events  
 277 is not always the same for the GPS data and for the tremor data, we identify the same  
 278 10 events in both 8th wavelet decompositions for the 8th level: Summer 2010, Summer  
 279 2011, Summer 2012, Fall 2013, Summer-Fall 2014, Winter 2015-2016, Winter 2017, Spring  
 280 2018, Spring-Fall 2019, and Fall 2020 - Winter 2021. We can also see the end of an 11th  
 281 event in Summer 2009.

282 Figures 7 and 8 show the same comparison between the wavelet decomposition of  
 283 the GPS data and the wavelet decomposition of the tremor count data for the 7th level  
 284 and the 6th level respectively. For the 7th level, we see the same events as for the 8th  
 285 level, both for the GPS data and the tremor count data. The wavelet decomposition is  
 286 more noisy for the GPS data in the earliest part of the time series, between 2010 and  
 287 2013, but it does not seem that there are more slow slip events visible in the 7th level.

288 For the 6th level detail, we see an additional event in Fall 2009 that is present both  
 289 in the GPS and the tremor data. There are three small signals in the GPS data in Spring  
 290 2012, Fall 2017, and Winter 2020 that are not present in the tremor data, and are prob-  
 291 ably false detections. To summarize, all the 11 events present on the 7th and 8th level  
 292 details of the wavelet decomposition are true detections, 12 of the 15 events present on  
 293 the 6th level detail of the wavelet decomposition are true detections.

## 294 5 Discussion

295 In addition to the magnitude 6 events discussed above, Michel, Gualandi, and Avouac  
 296 (2019) have also identified several magnitude 5 events using a variational Bayesian In-  
 297 dependent Component Analysis (vbICA) decomposition of the signal. As we expect smaller  
 298 magnitude events to be more visible at smaller time scales of the wavelet decomposi-  
 299 tion (levels 4 and 5), we verify for all these events whether a signal can be seen at the same  
 300 time as the time given in their catalog. Most of these magnitude 5 events are also sub-  
 301 events of bigger magnitude 6 events. Table 1 summarizes for each event its number as  
 302 indicated in the catalog from Michel et al. (2019), the beginning and end times as in-  
 303 dicated in the catalog from Michel et al. (2019), whether it is visible at the level 4 of  
 304 the wavelet decomposition, whether it is visible at the level 5 of the wavelet decompo-  
 305 sition, and whether it is part of a bigger magnitude 6 event. All 10 events that are sub-  
 306 event of a bigger event are visible at both levels 4 and 5. However, this may be due be-  
 307 cause the bigger event is in at levels 6 to 8, and also at smaller time scales. For the 3  
 308 small events that are not part of a bigger event, only one is visible at both time scales,  
 309 the other two are visible either for level either for level 5 of the wavelet decompositon.  
 310 Therefore, it is difficult to conclude whether the method can indeed detect events of mag-  
 311 nitude 5.

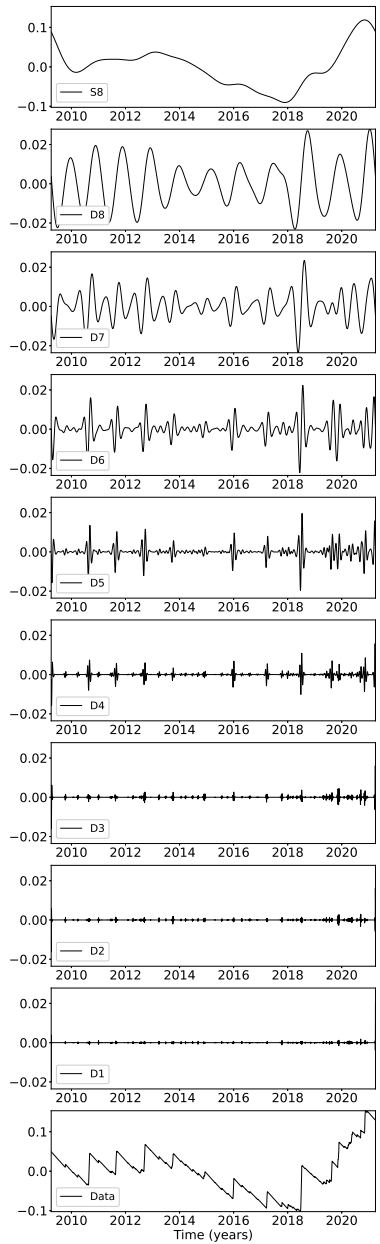


**Figure 5.** Details and smooth of the wavelet decomposition of the detrended cumulative tremor count around the third northernmost location on Figure 3.

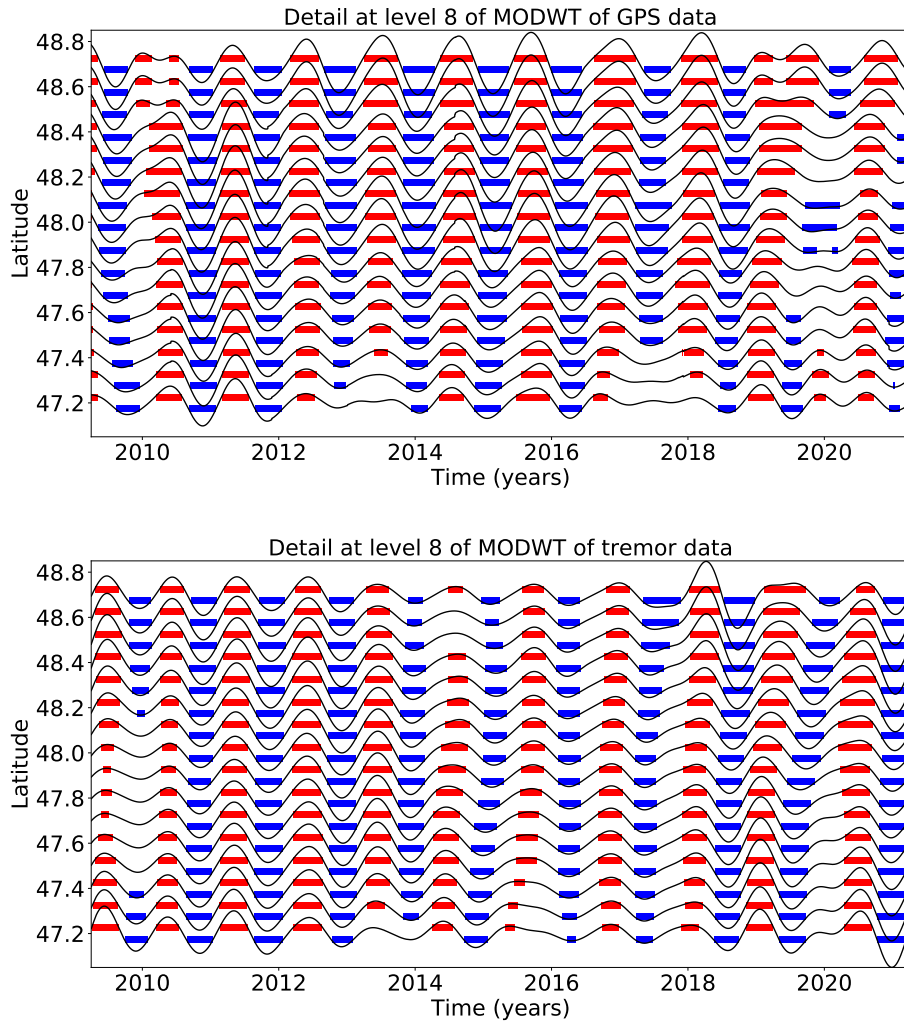


**Figure 6.** Top: Stacked 8th level details of the wavelet decomposition of the displacement over all the GPS stations located in a 50 km radius of a given point, for the 16 locations indicated in Figure 3. Bottom: Opposite of the 8th level detail of the cumulative tremor count in a 50 km radius of a given point for the same 16 locations.

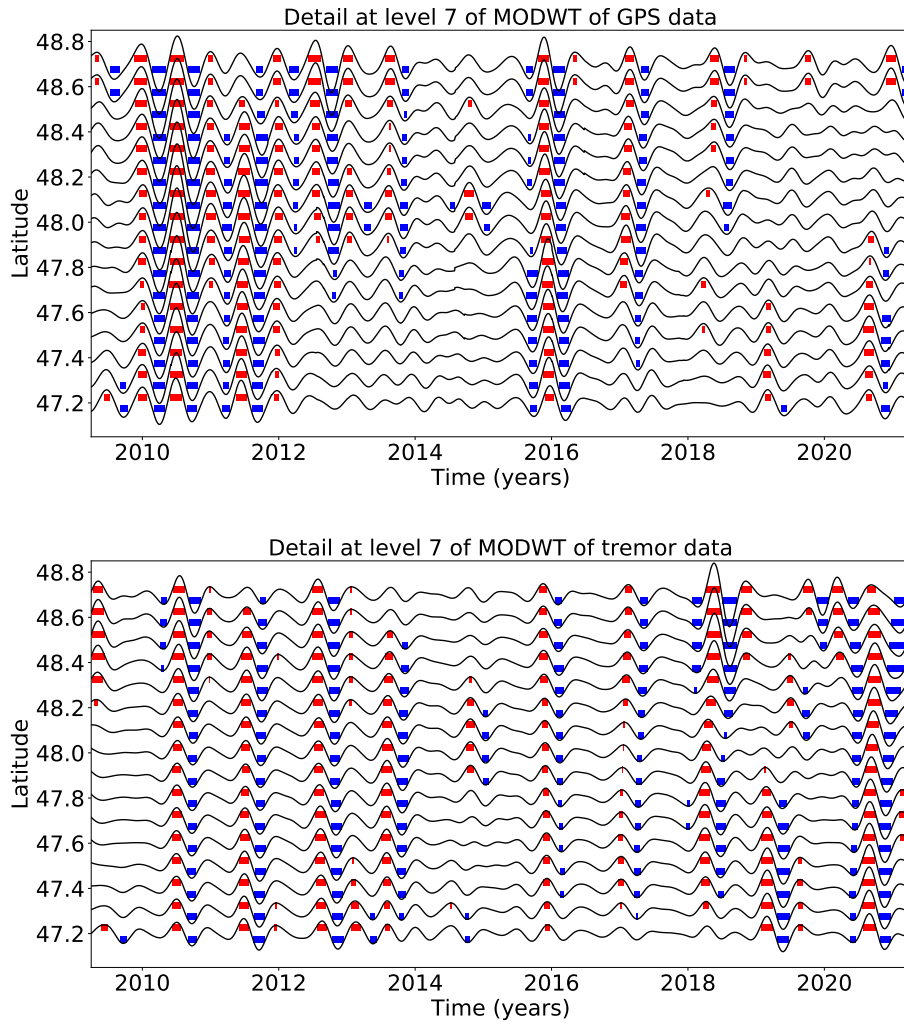


**Figure 7.** Top: Stacked 7th level details of the wavelet decomposition of the displacement over all the GPS stations located in a 50 km radius of a given point, for the 16 locations indicated in Figure 3. Bottom: Opposite of the 7th level detail of the cumulative tremor count in a 50 km radius of a given point for the same 16 locations.

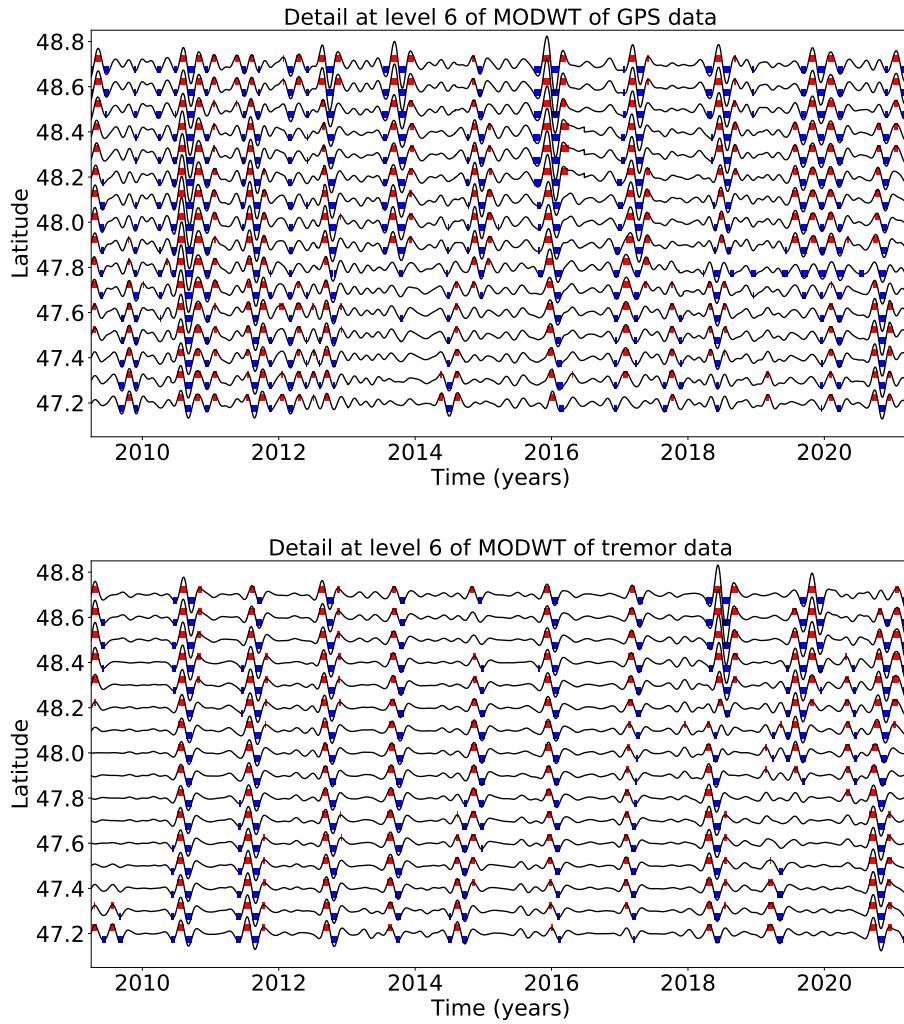


**Figure 8.** Top: Stacked 6th level details of the wavelet decomposition of the displacement over all the GPS stations located in a 50 km radius of a given point, for the 16 locations indicated in Figure 3. Bottom: Opposite of the 6th level detail of the cumulative tremor count in a 50 km radius of a given point for the same 16 locations.

**Table 1.** Magnitude 5 events from Michel et al. (2019).

Event number	Time	Visible at level 4	Visible at level 5	Sub-event of bigger event
25	2010.62-2010.67	Yes	Yes	Yes
29	2011.42-2011.45	No	Yes	No
31	2011.62-2011.68	Yes	Yes	Yes
32	2011.65-2011.68	Yes	Yes	Yes
35	2012.66-2012.72	Yes	Yes	Yes
42	2013.70-2013.78	Yes	Yes	Yes
44	2014.12-2014.20	Yes	No	No
45	2014.40-2014.48	Yes	Yes	No
49	2014.66-2014.71	Yes	Yes	Yes
52	2014.91-2014.95	Yes	Yes	Yes
57	2015.98-2016.08	Yes	Yes	Yes
60	2017.11-2017.15	Yes	Yes	Yes
61	2017.20-2017.24	Yes	Yes	Yes

## 312 6 Conclusion

### 313 Acknowledgments

314 Enter acknowledgments, including your data availability statement, here.

### 315 References

- 316 Aguiar, A., Melbourne, T., & Scrivner, C. (2009). Moment release rate of Cascadia  
317 tremor constrained by GPS. *Journal of Geophysical Research*, 114, B00A05.
- 318 Alba, S., Weldon, R. J., Livelybrooks, D., & Schmidt, D. A. (2019). Cascadia ETS  
319 events seen in tidal records (1980–2011). *Bulletin of the Seismological Society  
320 of America*.
- 321 Audet, P., & Kim, Y. (2016). Teleseismic constraints on the geological environ-  
322 ment of deep episodic slow earthquakes in subduction zone forearcs: A review.  
323 *Tectonophysics*, 670, 1-15.
- 324 Beroza, G., & Ide, S. (2011). Slow earthquakes and nonvolcanic tremor. *Annual Re-  
325 view of Earth and Planetary Sciences*, 39, 271-296.
- 326 Frank, W. (2016). Slow slip hidden in the noise: The intermittence of tectonic re-  
327 lease. *Geophysical Research Letters*, 43, 10125-10133.
- 328 Kumar, P., & Foufoula-Georgiou, E. (1997). Wavelet analysis for geophysical appli-  
329 cations. *Reviews of Geophysics*, 35(4), 385-412.
- 330 Michel, S., Gualandi, A., & Avouac, J.-P. (2019). Interseismic coupling and slow slip  
331 events on the Cascadia megathrust. *Pure and Applied Geophysics*, 176, 3867-  
332 3891.
- 333 Obara, K. (2002). Nonvolcanic deep tremor associated with subduction in southwest  
334 Japan. *Science*, 296(5573), 1679-1681.
- 335 Ohtani, R., McGuire, J., & Segall, P. (2010). Network strain filter: A new tool for  
336 monitoring and detecting transient deformation signals in GPS arrays. *Journal  
337 of Geophysical Research*, 115, B12418.
- 338 Percival, D., & Walden, A. (2000). *Wavelet Methods for Time Series Analysis*. New  
339 York, NY, USA: Cambridge University Press.
- 340 Preston, L., Creager, K., Crosson, R., Brocher, T., & Trehu, A. (2003). Intralab  
341 earthquakes: Dehydration of the Cascadia slab. *Science*, 302, 1197-1200.
- 342 Rogers, G., & Dragert, H. (2003). Tremor and slip on the Cascadia subduction zone:

- 343      The chatter of silent slip. *Science*, 300(5627), 1942-1943.
- 344      Shelly, D., Beroza, G., & Ide, S. (2007). Non-volcanic tremor and low-frequency  
345      earthquake swarms. *Nature*, 446, 305-307.
- 346      Szeliga, W., Melbourne, T., Miller, M., & Santillan, V. (2004). Southern Cascadia  
347      episodic slow earthquakes. *Geophysical Research Letters*, 31, L16602.
- 348      Szeliga, W., Melbourne, T., Santillan, M., & Miller, M. (2008). GPS constraints on  
349      34 slow slip events within the Cascadia subduction zone, 1997-2005. *Journal of*  
350      *Geophysical Research*, 113, B04404.
- 351      Wech, A. (2010). Interactive tremor monitoring. *Seismological Research Letters*,  
352      81(4), 664-669.
- 353      Wei, M., McGuire, J., & Richardson, E. (2012). A slow slip event in the south cen-  
354      tral Alaska Subduction Zone. *Geophysical Research Letters*, 39, L15309.